Torsten Wichtmann
Theodor Triantafyllidis

On the correlation of "static" and "dynamic" stiffness moduli of non-cohesive soils

The secant stiffness of the stress - strain - hysteresis during a cyclic or dynamic loading with very small strain amplitudes is sometimes called "dynamic" stiffness of a soil. In contrast, a "static" stiffness is obtained from the first loading curve in oedometric or triaxial tests. Indeed the difference between "dynamic" (small-strain) and "static" (large-strain) stiffness moduli is due to the different magnitude of strain or strain amplitude and not due to different loading rates. The small strain stiffness is an important design parameter for foundations subjected to a cyclic or dynamic loading. However, its determination in situ or from laboratory tests is laborious and expensive. In practice the small-strain stiffness is often estimated my means of a diagram correlating "dynamic" and "static" stiffness moduli. However, the assumptions and the range of applicability of this correlation are not clear. The present paper presents an inspection of this correlation for four sands with different grain size distribution curves. The "static" stiffness was obtained from tests with monotonic oedometric or triaxial compression. The "dynamic" stiffness was determined in resonant column tests and from measurements of the P-wave velocity. For some of the tested sands, significant deviations of the experimental data from the correlation actually used in practice were obtained. Modified correlations are proposed in the paper.

1 Introduction

A foundation subjected to a cyclic loading (quasi-static or dynamic) has to be designed with regard to the short-term *and* the long-term behaviour. The long-term behaviour (accumulation of residual deformations or stress relaxation) has been discussed in [1–4]. The present paper concentrates on the short-term behaviour, where the soil properties are assumed not to change during the cycles.

For an analysis of the short-term behaviour of a foundation a one-dimensional model with a mass, a spring and a dashpot is often used (e.g. [5–7]). The elastic constants of the soil enter the equations for the parameters of the spring and the dashpot. Usually the formulas use the shear stiffness G and Poisson's ratio ν as input parameters. Since the loading is of a cyclic nature, the secant shear stiffness G_{sec} of the shear stress - shear strain hystereses (Fig. 1a) has to be used for G as an average value.
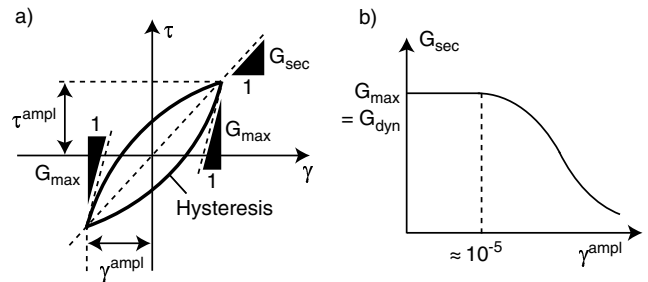

Fig. 1: *a) Definition of the secant shear stiffness G_{sec} of the τ-γ-hysteresis, b) Decrease of G_{sec} from its maximum value $G_{\max}$ with increasing shear strain amplitude γ^{ampl}*

For a non-cohesive soil the secant shear stiffness G_{sec} does not depend on the shear strain amplitude up to a threshold value of $\gamma^{\text{ampl}} \approx 10^{-5}$. For larger shear strain amplitudes, G_{sec} decreases with increasing γ^{ampl} (Figure 1b). The maximum value $G_{\max} = G_{\text{dyn}}$ at very small strain amplitudes is sometimes called "dynamic" shear modulus. However, this terminology is somewhat misleading since the secant stiffness G_{sec} does not depend on the frequency of excitation. In the case of small shear strain amplitudes $\gamma^{\text{ampl}} < 10^{-5}$ the maximum value $G_{\max}$ can be directly set into the equations for the spring and dashpot parameters. For larger amplitudes it has to be reduced by a factor $G_{\text{sec}}/G_{\max} < 1$ [8,9].

The small-strain shear modulus $G_{\max}$ of a non-cohesive soil can be determined using different methods, with different effort and accuracy:

1. In-situ measurements of the shear wave velocity $v_S = \sqrt{G_{\max}/\varrho}$, where ϱ is the density of the soil (e.g. cross-hole measurements).

2. Laboratory tests (e.g. resonant column tests or measurements of the S-wave velocity in a triaxial cell). However, specimens reconstituted in the laboratory may not reproduce the in-situ fabric of the grain skeleton. Furthermore, the shear stiffness measured in the laboratory is not influenced by aging or preloading effects. These effects may lead to an increase of $G_{\max}$ in situ [10]. Thus, laboratory tests usually under-estimate the in-situ values of $G_{\max}$. In the literature, it is discussed controversially if a (very expensive) sampling by means of freezing preserves the fabric of the soil. If the fab-

ric is preserved in these samples the shear moduli measured in the laboratory should better coincide with the in-situ G_{max}-values.

3. Rough estimation of G_{max} by means of tables which specify a range of stiffness moduli for various types of soil (see e.g. [7]). Since the range of the recommended values is quite large and no information about the (important) stress level is given, the reader is advised not to use these tables.

4. Estimation of G_{max} from empirical equations. The formula most commonly used was developed by Hardin [11, 12] and is also recommended in [7]:

$$G_{max}[\text{MPa}] \quad = \quad A\,\frac{(a-e)^2}{1+e}\,(p[\text{kPa}])^n \quad (1)$$

Therein e and p are the void ratio and the mean effective pressure, respectively. The constants A, a and n proposed by Hardin [11, 12] depend only on the grain shape ($A = 6.9$, $a = 2.17$ and $n = 0.5$ for round grains and $A = 3.2$, $a = 2.97$ and $n = 0.5$ for angular grains).

However, tests on sands with different grain size distribution curves [13–15] show that G_{max} strongly decreases with increasing coefficient of uniformity $C_u = d_{60}/d_{10}$. In contrast, there is no influence of the mean grain size d_{50}, at least for materials in the range of fine sands to fine gravels. An increase of G_{max} with d_{50} for gravelly materials is reported e.g. in [16]. While Eq. (1) delivers acceptable G_{max}-values for poorly-graded grain size distribution curves, the shear moduli of sands with higher C_u-values may be strongly over-estimated (by up to 100 %, see [9, 15]).

Based on 163 RC tests on 25 different grain size distribution curves, correlations of the constants A, a and n in Eq. (1) with C_u have been proposed in [15]. As demonstrated in [15], the predictions using Hardin's equation and these new correlations are in good accordance with the test data for the various grain size distribution curves.

5. Use of a correlation diagram as given in Fig. 2. It shows the ratio of small strain ("dynamic") and large-strain ("static") stiffness moduli as a function of the static values.

The single curve originally proposed by Alpan [17] (Fig. 2) describes the relationship between "static" and "dynamic" Young's moduli (E_{stat}, $E_{dyn} = E_{max}$). The static values are obtained from triaxial test data. The meaning of the "static" modulus has been discussed controversially in [18, 19]. From [17] it does not become clear if "static" Young's modulus means the stiffness during first loading (e.g. E_{50}, defined as the inclination of the initial phase of the curve $q(\varepsilon_1)$ up to $0.5q_{max}$, Fig. 3) or the secant stiffness during a large un- and re-loading cycle (E_{ur}, Fig. 3). Benz & Vermeer [18] argued for E_{ur}.
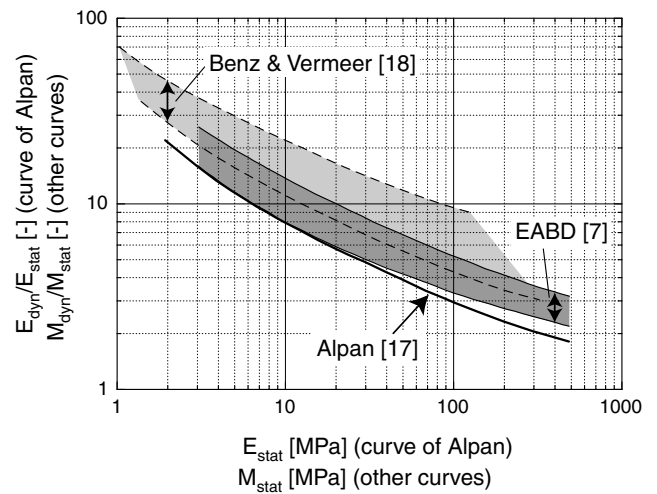

Fig. 2: *Comparison of the correlation $E_{dyn}/E_{stat} \leftrightarrow E_{stat}$ of Alpan [17] with the correlations $M_{dyn}/M_{stat} \leftrightarrow M_{stat}$ given in [7] and by Benz & Vermeer [18]*

However, Alpan [17] introduced the tangent elastic modulus E_i as the inclination of the nearly linear initial portion of the q-ε_1-curve, i.e. as a stiffness for first loading (similar to E_{50}). Tests with un- and reloading cycles are not discussed in [17], that means a secant modulus E_{ur} as shown in Fig. 3 has not been defined by Alpan [17]. For the abovementioned reasons it can be assumed that Alpan [17] considers $E_{stat} \approx E_{50}$. However, the experimental data presented later in this paper supports the assumption $E_{stat} = E_{ur}$ (Section 4.3). A diagram showing the curve of Alpan is also printed in [20] but the axes labels are erroneous.
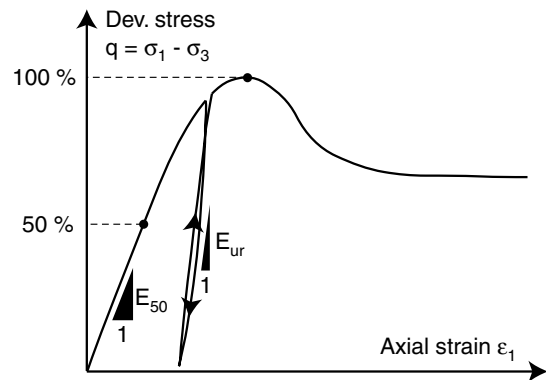

Fig. 3: *Scheme of a curve $q(\varepsilon_1)$ in a monotonic triaxial test with an un- and reloading cycle, definition of E_{50} and E_{ur}*

In [7] the correlation between dynamic and static stiffness moduli is given in terms of the modulus M for one-dimensional compression (zero lateral strain). The relationship is also shown in Fig. 2, where the ratio $M_{dyn}/M_{stat} = M_{max}/M_{stat}$ is plotted as a function of M_{stat}. The correlation has been derived from the curve of Alpan [17], but in contrast to that curve, [7] provides upper and lower boundaries for different types of soils. No testing proce-

2

dure for the determination of M_{stat} is prescribed in [7]. Since no un- and reloading cycles are mentioned in [7], the input parameter M_{stat} is probably meant as the stiffness modulus during first loading. According to our experience, the diagram is used in this way in practice.

Benz & Vermeer [18] provide an alternative correlation $M_{dyn}/M_{stat} \leftrightarrow M_{stat}$ (see Fig. 2). It is also based on the curve of Alpan [17]. For a given value of M_{stat}, the ratios M_{dyn}/M_{stat} predicted by the correlation of Benz & Vermeer [18] lay significantly higher than those obtained from the relationship recommended in [7]. This is probably due to a different interpretation of Alpan's E_{stat} ($E_{stat} = E_{ur} \approx 3E_{50}$ in [18], $E_{stat} = E_{50}$ in [7]).

Having determined $E_{max} = E_{dyn}$ or $M_{max} = M_{dyn}$ from Fig. 2, the small strain shear modulus G_{max} may be obtained with an estimated Poisson's ratio ν:

$$G_{max} = E_{max} \frac{1}{2(1+\nu)} = M_{max} \frac{1 - \nu - 2\nu^2}{2(1-\nu^2)} \quad (2)$$

The method using Fig. 2 is often applied in practice since for many in-situ soils M_{stat}-values from oedometric tests are available. Furthermore, in the laboratory a determination of M_{stat} is much less laborious and less expensive than the measurement of G_{max}.

However, in [17] and [7] it is not specified for which stresses, densities, grain shapes or grain size distribution curves the correlations $E_{dyn}/E_{stat} \leftrightarrow E_{stat}$ or $M_{dyn}/M_{stat} \leftrightarrow M_{stat}$, respectively, have been developed. Thus, the range of applicability is not clear.

The aim of the present paper is the inspection of the correlations given in Fig. 2. Different laboratory tests on four sands with different grain size distribution curves have been performed, in particular:

- Monotonic oedometric compression tests for M_{stat}
- Monotonic triaxial compression tests for E_{stat}
- Measurements of the P-wave velocity v_P during isotropic compression of triaxial specimens for $M_{max} = M_{dyn}$
- Resonant Column (RC) tests for $G_{max} = G_{dyn}$

The results and possible correlations are discussed in the following.

2 Tested materials

The grain size distribution curves of the four tested sands are shown in Fig. 4. Three of them (Nos. 1,2,3) were poorly-graded ($1.4 \leq C_u = d_{60}/d_{10} \leq 2.0$) with different mean grain sizes $0.21 \leq d_{50} \leq 1.45$ mm. The fourth sand was well-graded ($C_u = 4.5$, $d_{50} = 0.52$ mm). All grain size distribution curves lay in the range between fine sand and fine gravel. Table 1 summarizes the values of d_{50}, C_u and the minimum and maximum void ratios e_{min} and e_{max} of the tested materials.
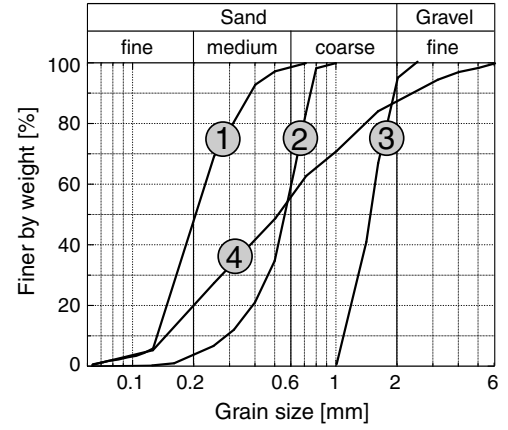

Fig. 4: *Grain size distribution curves of the four tested sands*

Sand No.	d_{50} [mm]	C_u [-]	e_{min} [-]	e_{max} [-]
1	0.21	2.0	0.575	0.908
2	0.55	1.8	0.577	0.874
3	1.45	1.4	0.623	0.886
4	0.52	4.5	0.422	0.691

Table 1: Mean grain size d_{50}, coefficient of uniformity $C_u = d_{60}/d_{10}$, minimum (e_{min}) and maximum (e_{max}) void ratio according to DIN 18126 [21] for the four tested sands

3 Test results
3.1 Large-strain modulus M_{stat} from oedometric compression tests

The 28 oedometric tests were performed using large specimens (diameter $d = 28$ cm, height $h = 8$ cm, ratio $d/h = 3.5$) in order to improve the repeatability of the tests on the coarser soils. The test device is shown in Fig. 5. The stiff lateral ring of the specimen is fixed. The top cap of the specimen and the load piston are rigidly connected. The load piston is guided in the vertical direction by a ball bearing. The axial load is applied to the load piston by means of a pneumatic cylinder and a lever arm loading system. The axial load is measured by means of a load cell located at the top of the load piston. The axial deformation Δh of the specimen is measured with a displacement transducer attached to the load piston. Comparative tests with the finest tested sand No. 1 in a standard device with small specimen dimensions ($d = 7$ cm, $h = 2$ cm) showed similar results as the tests with the large specimens.

The lateral stress σ_3 could not be measured. It was estimated from the vertical stress σ_1 using the relationship $\sigma_3 = K_0 \sigma_1$. The coefficient of lateral stress was estimated as $K_0 = 1 - \sin \varphi_P$ according to Jaky. φ_P is the peak friction angle which depends primary on the density of the soil. φ_P was determined from the monotonic triaxial tests (Section 3.2).

For each sand several oedometric tests with different initial relative densities $I_{D0} = (e_{max} - e)/(e_{max} - e_{min})$ were performed. Specimens were prepared by dry plu-
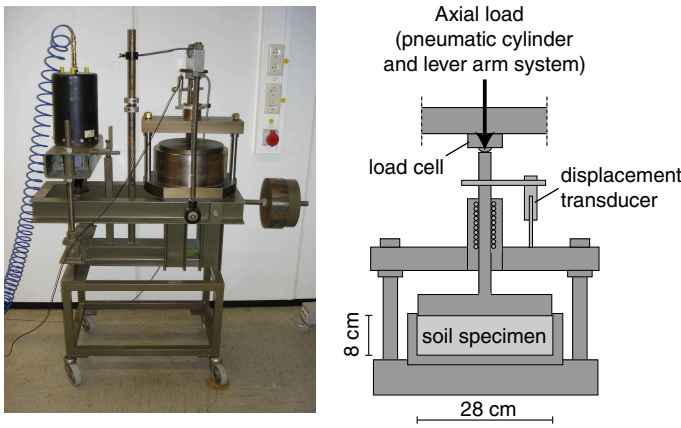
Fig. 5: *Test device for oedometric compression (specimen size d = 28.0 cm, h = 8 cm)*

viation and were tested in the dry condition. The axial stress was increased in 15 steps up to a maximum value of $\sigma_1 = 800$ kPa. The reduction of void ratio e with increasing mean pressure $p = (\sigma_1 + 2\sigma_3)/3$ is shown exemplary for a loose and a dense specimen of sand No. 2 in Fig. 6.
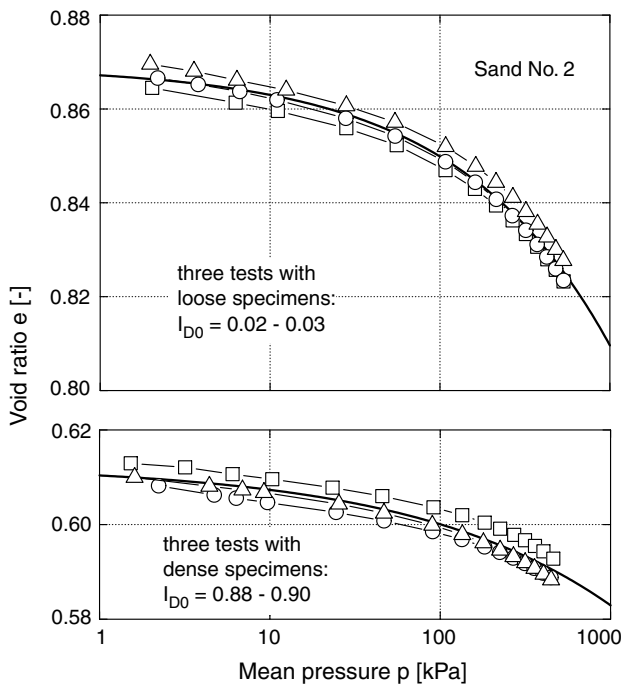

Fig. 6: *Reduction of void ratio e with mean pressure p in oedometric tests on sand No. 2*

For a certain load step, M_{stat} is determined as the secant modulus from the increment of the axial stress $\Delta\sigma_1$, the increment of void ratio Δe and the void ratio e_0 prior to the load step [22]:

$$M_{stat} = \frac{\Delta\sigma_1}{\Delta e}(1 + e_0) \qquad (3)$$

This is equivalent to $M_{stat} = \Delta\sigma_1/\Delta\varepsilon_1$ if the increment of axial strain $\Delta\varepsilon_1 = \Delta h/h_0$ is calculated with h_0 being the height of the specimen prior to the load step.

The diagrams in the left column in Fig. 7 (diagrams a-d) present M_{stat} as a function of void ratio e for seven different mean pressures 50 kPa $\leq p \leq$ 400 kPa. The data for a certain p was obtained from an interpolation between two adjacent p-values where data was available. An approximation of M_{stat} by a a unique formula describing stress- and void ratio-dependence simultaneously (i.e. analogously to Eq. (1)) was found to be inaccurate. Thus, the function

$$M_{stat} = A \frac{(a-e)^2}{1+e} \qquad (4)$$

with constants A (unit [MPa]) and a was fitted separately to the data for each pressure p. The constants A and a are summarized in Table 2. The solid curves in Fig. 7a-d were generated using Eq. (4) with the constants A and a taken from Table 2.

Fig. 8 compares the stiffness moduli M_{stat} of the four tested sands for a pressure $p = 200$ kPa. For an identical void ratio, the poorly-graded sands Nos. 1 to 3 have significantly larger M_{stat}-values compared to the well-graded sand No. 4. For the poorly-graded sands the M_{stat}-values coincide for larger void ratios $e \approx 0.8$. For smaller void ratios, M_{stat} increases with decreasing mean grain size d_{50}.
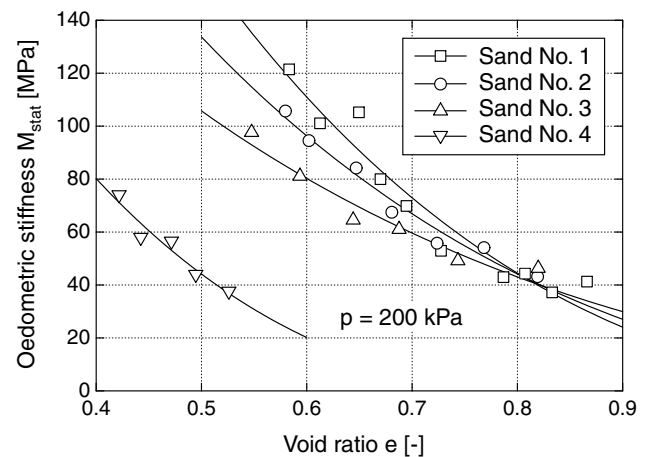

Fig. 8: *Oedometric stiffness $M_{stat}(e)$ of the four tested sands at p = 200 kPa*

3.2 Large-strain modulus E_{stat} and peak friction angle φ_P from monotonic triaxial tests

The 30 monotonic triaxial tests were performed for two different reasons. First, a modulus $E_{stat} = E_{50}$ is obtained from the initial phase of a test. Second, the peak friction angle φ_P is necessary to analyze the oedometric tests presented in Section 3.1 (in order to estimate the lateral stress σ_3 and to calculate p).

For each sand, two or three test series differing in the initial relative density I_{D0} were performed. For each density, three different effective lateral stresses were tested ($\sigma_3 = 50$, 100 and 200 kPa). Specimens were prepared by pluviating dry sand out of a funnel. Afterwards
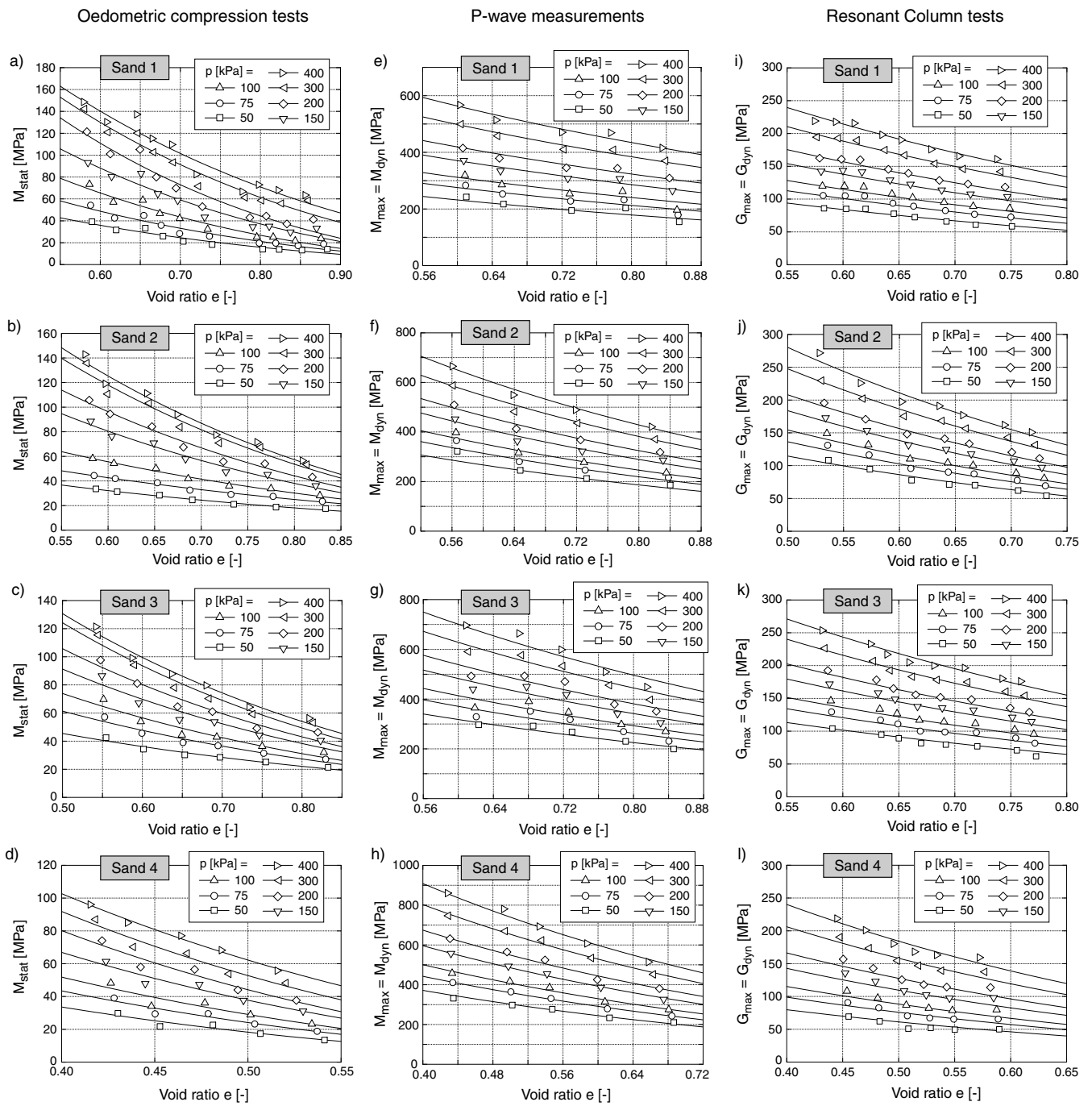
Oedometric compression tests   P-wave measurements   Resonant Column tests

Fig. 7: *Stiffness moduli M_{stat} from oedometric tests, $M_{\max} = M_{dyn}$ from P-wave measurements and $G_{\max} = G_{dyn}$ from resonant column tests as a function of void ratio e and mean pressures p*

p	Sand No. 1		Sand No. 2		Sand No. 3		Sand No. 4	
	A	a	A	a	A	a	A	a
50	53.5	1.58	125.3	1.28	42.4	1.77	263.3	0.82
75	60.6	1.66	176.6	1.26	73.9	1.62	317.5	0.84
100	106.3	1.51	270.9	1.22	103.2	1.54	366.7	0.84
150	235.9	1.34	342.6	1.24	128.0	1.53	463.6	0.85
200	305.6	1.31	478.8	1.21	159.6	1.50	604.1	0.83
300	382.7	1.30	382.9	1.34	198.1	1.47	597.0	0.86
400	400.6	1.31	337.9	1.41	190.6	1.51	542.6	0.91

Table 2: Summary of constants A (in [MPa]) and a in Eq. (4) for the four tested sands

they were saturated with de-aired water. The drained monotonic triaxial compression was applied with a constant displacement rate of 0.1 mm/min in the axial direction. The axial load, the axial displacement and the volume changes (via the pore water using a pipette system and a differential pressure transducer) were measured. The test device and the method of specimen preparation is explained in detail in [2].

Typical curves of deviatoric stress $q = \sigma_1 - \sigma_3$ as a function of axial strain ε_1 are given in Fig. 9. At $q = 0$ the curves should start with an inclination corresponding to $E_{max} = E_{dyn}$. However, this part of the curve can hardly be measured in a monotonic triaxial test using standard equipment. With increasing strain, the inclination of the curves decreases, i.e. the curves are non-linear. A common approximation of the inclination of the initial part of the $q(\varepsilon_1)$-curve is the secant Young's modulus E_{50} defined as

$$E_{50} = \frac{q_{50}}{\varepsilon_{1,50}} \tag{5}$$

with the half peak deviatoric stress $q_{50} = q_{peak}/2$ and the corresponding axial strain $\varepsilon_{1,50}$ (see Fig. 9). The system compliance of the triaxial device was determined in a preliminary test with a steel dummy. It was subtracted from the measured axial deformation. Thus, the values $\varepsilon_{1,50}$ used for the calculation of E_{50} are free from system compliance.
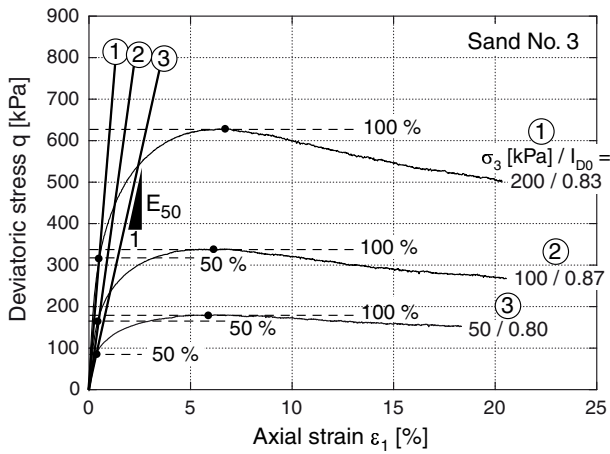

Fig. 9: *Curves $q(\varepsilon_1)$ in drained monotonic triaxial tests on sand No. 3, determination of E_{50}*

For each test, the Young's modulus E_{50} was determined according to Eq. (5). In Fig. 10 it is plotted versus the void ratio $(e_0 + e_{50})/2$, which is the mean value of the void ratios at $q = 0$ and $q = q_{50}$. Obviously, E_{50} increases with decreasing void ratio and with increasing lateral effective stress σ_3.

Fig. 11 presents the peak stress states in the p-q-plane. For each density, the data of the three different σ_3-values was approximated by a linear curve, passing the origin with the inclindation $M_c(\varphi_P) = 6 \sin \varphi_P / (3 - \sin \varphi_P)$. The peak friction angle was calculated from the M_c-value. In Fig. 12, φ_P is plotted versus the void ratio
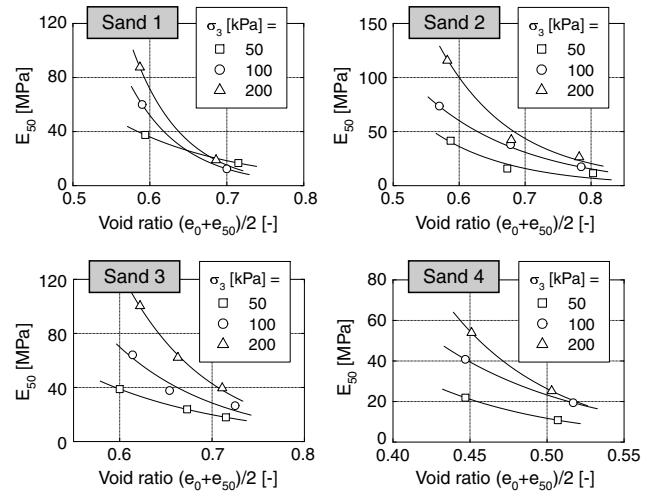

Fig. 10: *Young's modulus E_{50} as a function of void ratio $(e_0 + e_{50})/2$*

e_P at peak (mean value of the three tests). Assuming $\varphi_P \approx \varphi_c$ for $e = e_{max}$ with φ_c being the critical friction angle, the function

$$\varphi_P = \varphi_c \exp \left(a_\varphi \left(e_{max} - e_P \right)^{b_\varphi} \right) \tag{6}$$

was fitted to the data in Fig. 12. The constants a_φ and b_φ are summarized in Table 3. The critical friction angle φ_c given in Table 3 was determined in separate tests as the inclination of a pluviated cone of sand.
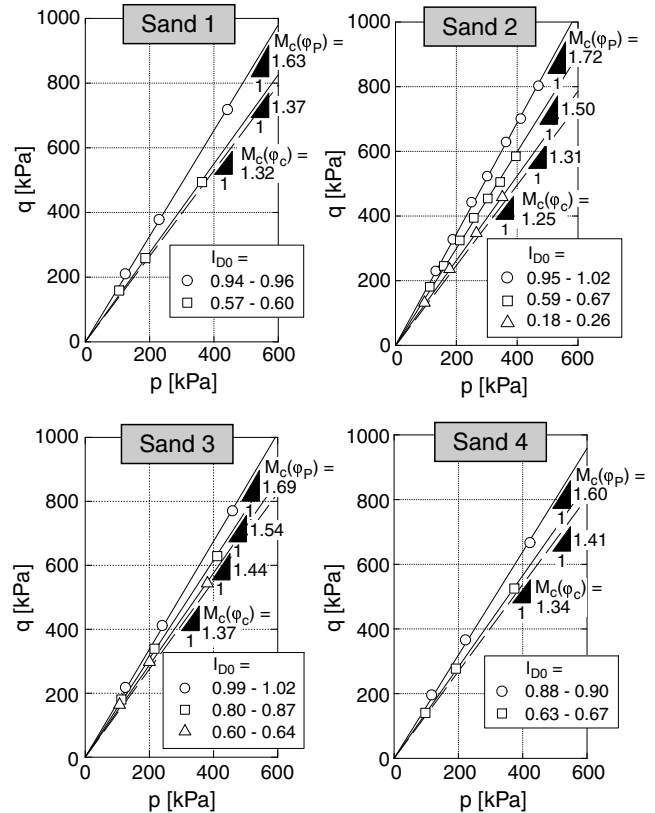

Fig. 11: *Peak stress states in the p-q-plane for the four tested sands and different initial densities I_{D0}*
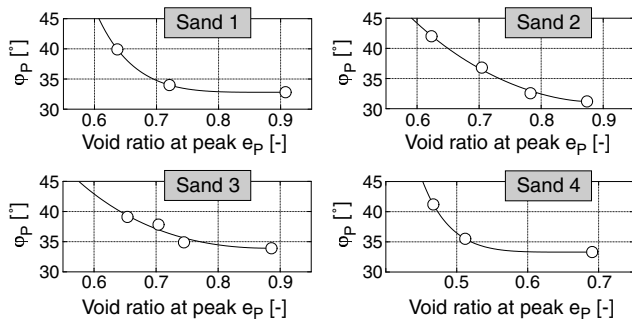
Fig. 12: *Peak friction angle φ_P in dependence on peak void ratio e_P for the four tested sands, fitting of Eq. (6)*

Sand No.	φ_c [°]	a_φ [-]	b_φ [-]
1	32.8	78.9	4.6
2	31.2	3.0	1.7
3	33.9	3.8	2.2
4	33.3	648	5.4

Table 3: *Critical friction angle φ_c, constants a_φ and b_φ of Eq. (6)*

3.3 Small-strain constrained elastic modulus $M_{\max} = M_{\mathbf{dyn}}$ from P-wave measurements

The P-wave velocity v_P correlates with the maximum constrained elastic modulus $M_{\max} = M_{\mathrm{dyn}}$ via $v_P = \sqrt{M_{\max}/\varrho}$. The P-wave velocity was measured in a triaxial cell by means of piezoelectric elements (Fig. 13). A single sinusoidal signal was generated by a function generator. It was amplified and applied to the piezoelectric element in the end plate at the bottom of the specimen. The distortion of the element in the vertical direction generates a P-wave travelling through the specimen and causing a distortion of the piezoelectric element in the top cap. This distortion generates an electrical signal. Both, the transmitted and the received signal are displayed on an oscilloscope. The travel time t_t of the wave is the time difference between the initial of both signals. Knowing the height h of the specimen, the P-wave velocity is calculated from $v_P = h/t_t$. The test device and the measuring technique is explained in detail in [2, 9].

In total, 19 tests with P-wave measurements were performed. For each sand several tests with different initial relative densities were conducted. The specimens were prepared by the pluviation technique. The isotropic stress ($p = \sigma_1 = \sigma_3$) was increased in seven steps ($p = 50, 75, 100, 150, 200, 300$ and 400 kPa). The P-wave measurements at a certain stress level were taken after a resting period of 15 minutes under this pressure. The axial deformation of the dry specimens was measured with a displacement transducer. Lateral deformations were measured by means of non-contact displacement transducers. For this purpose, aluminium targets were glued to the rubber membrane of the specimen. The diagrams in the middle column in Fig. 7

(diagrams e-h) present the stiffness $M_{\max}$ as a function of mean pressure p and void ratio e. Obviously, $M_{\max}$ increases with increasing p and with decreasing e.

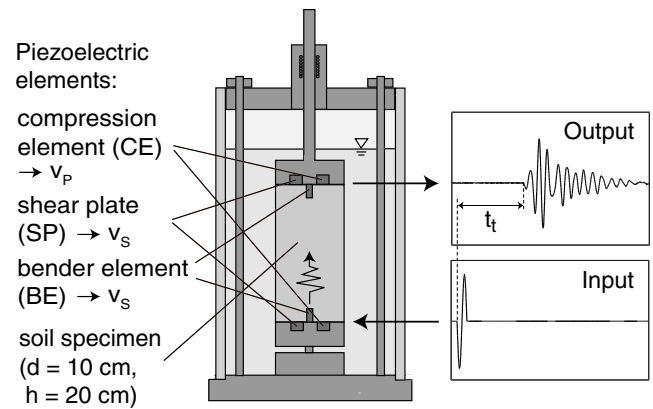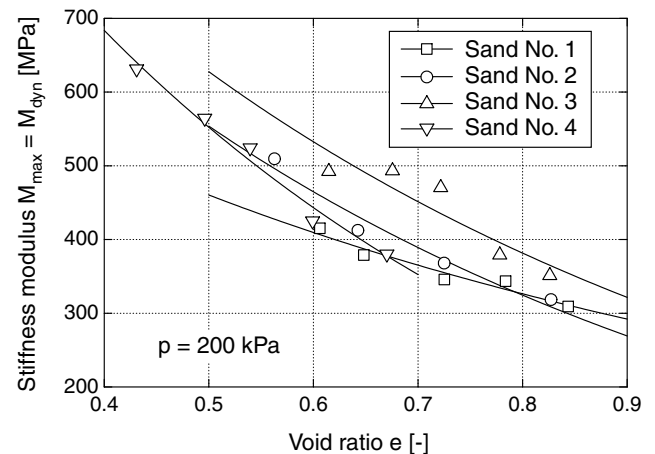Fig. 13: *Triaxial device with piezoelectric elements for the measurement of P- and S-wave velocities*

Fig. 14: *Modulus $M_{\max}(e) = M_{dyn}(e)$ of the four tested sands at $p = 200$ kPa*

Fig. 14 compares the curves $M_{\max}(e)$ of the four sands at pressure $p = 200$ kPa. In contrast to $G_{\max}$ (Section 3.4), the stiffness moduli $M_{\max}$ of the four sands almost coincide for $e = $ constant. The $M_{\max}$-values of the coarse sand No. 3 are somewhat larger than those of the other three sands. However, there is no significant influence of the grain size distribution curve on $M_{\max}$.

The empirical equation (analogously to Eq. (1), but with dimensionless constants)

$$M_{\max} = A_E \frac{(a_E - e)^2}{1 + e} p_{\mathrm{atm}}^{1-n_E} p^{n_E} \qquad (7)$$

with the atmospheric pressure $p_{\mathrm{atm}} = 100$ kPa was fitted to the data $M_{\max}(e, p)$. The constants A_E, a_E and n_E are summarized in Table 4. The solid curves in Fig. 7e-h were generated using Eq. (7) with the constants of Table 4. The predictions coincide well with the test data.

Sand No.	A_E [-]	a_E [-]	n_E [-]	A_G [-]	a_G [-]	n_G [-]
1	585	3.52	0.43	1196	1.84	0.45
2	1820	2.36	0.40	2513	1.46	0.43
3	1914	2.46	0.38	1288	1.90	0.42
4	3074	1.91	0.43	1409	1.47	0.53

Table 4: Constants A_E, a_E and n_E of Eq. (7) and constants A_G, a_G and n_G of Eq. (8) for the four tested sands

3.4 Small-strain shear modulus $G_{\max} = G_{\mathbf{dyn}}$ from resonant column (RC) tests

The small-strain shear modulus $G_{\max} = G_{\mathrm{dyn}}$ was measured in 29 resonant column (RC) tests. The test device is shown in Fig 15. It has been explained in detail in [2,9]. The nearly isotropic stress (a small anisotropy results from the weight of the top mass [9]) was increased in seven steps ($p = 50$, 75, 100, 150, 200, 300 and 400 kPa). At each stress level, the small-strain shear modulus was measured after a resting period of 15 minutes. The compaction of the specimen due to the increase of cell pressure was measured with non-contact displacement transducers.
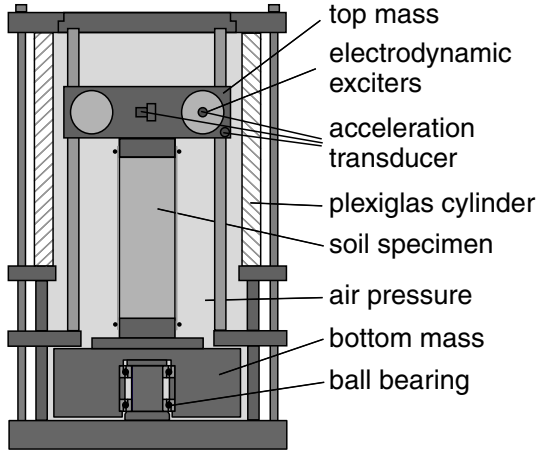

Fig. 15: *Scheme of the resonant column (RC) device*

The diagrams i-l in the right column in Fig. 7 present the small-strain shear modulus of the four sands as a function of void ratio e and mean pressure p. The curves $G_{\max}(e)$ for $p = 200$ kPa are compared in Fig. 16. In accordance with earlier test results [14] and also with our latest experimental studies [15], for $e, p = $ constant the small strain shear modulus does not depend on the mean grain size d_{50} but significantly decreases with increasing coefficient of uniformity $C_u = d_{60}/d_{10}$ of the grain size distribution curve. The largest $G_{\max}$-values were obtained for sand No. 3 with $C_u = 1.4$. Somewhat smaller values were measured for sands Nos. 1 and 2 with $C_u = 1.8 \div 2.0$ (confirming the d_{50}-independence of $G_{\max}$). The lowest $G_{\max}$-values were observed for sand No. 4 with the largest C_u-value ($C_u = 4.5$).

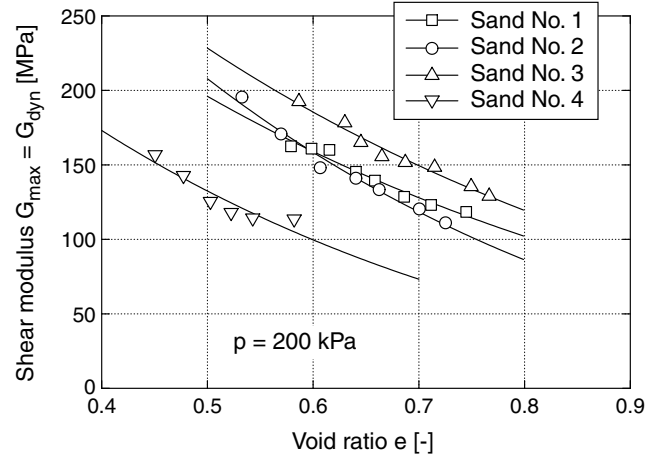The small-strain shear modulus $G_{\max}(e, p)$ was ap-

Fig. 16: *Small-strain shear modulus $G_{\max}(e) = G_{dyn}(e)$ for the four tested sands at $p = 200$ kPa*

proximated by a dimensionless version of Eq. (1):

$$G_{\max} = A_G \, \frac{(a_G - e)^2}{1 + e} \, p_{\mathrm{atm}}^{1-n_G} \, p^{n_G} \qquad (8)$$

The constants A_G, a_G and n_G are given in Table 4. The solid curves in Fig. 7i-l were generated using Eq. (8) and the constants in Table 4. A good congruence between measured and predicted $G_{\max}$-values can be stated.

3.5 Poisson's ratio ν

Unfortunately, measurements of the S-wave velocity in the triaxial cell, Section 3.3, have not been performed. However, the shear wave velocity $v_S = \sqrt{G_{\max}/\varrho}$ obtained from a resonant column test and v_S directly measured with piezoelectric elements are almost identical [9]. Thus, v_S from the RC tests (Section 3.4) and v_P from the measurements with piezoelectric elements (Section 3.3) may be used to calculate Poisson's ratio ν:

$$\nu = \frac{2 - (v_P/v_S)^2}{2 - 2 (v_P/v_S)^2} \qquad \text{or} \qquad (9)$$

$$\nu = \frac{\alpha}{4(1-\alpha)} + \sqrt{\left(\frac{\alpha}{4(1-\alpha)}\right)^2 - \frac{\alpha-2}{2(1-\alpha)}}, (10)$$

respectively, with $\alpha = M_{\max}/G_{\max}$.

Eq. (10) was evaluated with $M_{\max}$ and $G_{\max}$ calculated from Eqs. (7) and (8) with the constants in Table 4. The resulting Poisson's ratios are shown in Fig. 17 in dependence of void ratio e and mean pressure p. For all tested sands ν increases with e. This increase is more pronounced for the poorly-graded fine and medium coarse sands. The slight stress-dependence results from the moderately different values of the constants n_E and n_G in Eqs. (7) and (8) (Table 4). For the poorly-graded sands Nos. 1 to 3 the Poisson's ratios lay in the range $0.18 \leq \nu \leq 0.37$. These values coincide with typical ν-values ($0.25 \leq \nu \leq 0.35$) specified in [7] for sand and gravel. For the well-graded sand No. 4 higher ν-values ($0.34 \leq \nu \leq 0.43$) were obtained.
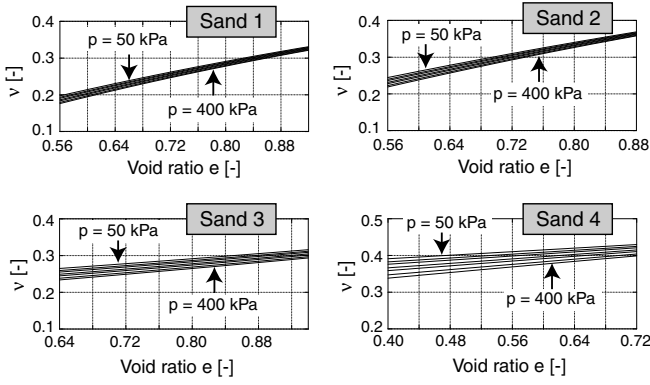
Fig. 17: *Poisson's ratio ν as a function of void ratio e and mean pressure p for the four tested sands*

If $G_{\max}$ is calculated from $M_{\max}$ or $E_{\max}$ (e.g. obtained from Fig. 2) using Eq. (2), the uncertainty resulting from an inaccurate estimation of the Poisson's ratio may be significant. Assuming $\nu = 0.2$ one obtains $G_{\max} = 0.375\, M_{\max}$ while $G_{\max} = 0.167\, M_{\max}$ results if Poisson's ratio is estimated as $\nu = 0.4$ (factor 2.2 difference). The diagrams in Fig. 17 may be used for a more accurate estimation of Poisson's ratio.

4 Inspection of various correlations of "dynamic" and "static" stiffness moduli

4.1 Correlation of M_{stat} with $M_{dyn} = M_{max}$

Using the results of the oedometric tests (Section 3.1) and the P-wave measurements (Section 3.3), the diagrams given in Fig. 18 were prepared. Similar to Fig. 2, Fig. 18 presents the ratio M_{dyn}/M_{stat} as a function of M_{stat}. A pair of values of M_{stat} and M_{dyn} was calculated from Eqs. (4) and (7) for the same mean pressure p and the same void ratio e. It should be considered that the stress is anisotropic ($\sigma_1 > \sigma_3$) in the oedometric tests while it was isotropic ($\sigma_1 = \sigma_3$) in the tests with the P-wave measurements. However, a stress anisotropy affects the "dynamic" stiffness only for stress ratios σ_1/σ_3 near failure [23]. Thus, it seems justified to compare M_{stat} and M_{dyn} for the same p. The relationship $M_{dyn}/M_{stat} \leftrightarrow M_{stat}$ was analyzed for a range of void ratios given in Fig. 18. Two neighboured data points have a distance $\Delta e = 0.01$.

Comparing the ratios M_{dyn}/M_{stat} of the poorly graded sands Nos. 1, 2 and 3 for a certain M_{stat}, the ratio M_{dyn}/M_{stat} increases with increasing mean grain size d_{50}. In Fig. 18, the range of the correlation recommended in [7] is marked by the dark-gray background color. For the fine and medium coarse sand No. 1 the measured values M_{dyn}/M_{stat} lay within this range, in particular for the higher stresses and lower void ratios (i.e. for larger values of M_{stat}). For the medium and coarse sand No. 2, the values M_{dyn}/M_{stat} lay at the upper boundary of the gray-colored area. For the coarse sand No. 3, the experimentally obtained data exceeds the range recommended in [7]. For the well-graded sand No. 4, the bandwidth specified in [7] strongly underes-

timates the experimentally obtained ratios M_{dyn}/M_{stat} (factor 1.5 to 3).

Thus, based on Fig. 18, the correlation given in [7] seems applicable only for poorly-graded fine and medium coarse sands. The small-strain stiffness of poorly-graded coarse sands and that of well-graded sands may be strongly underestimated by this correlation.

The correlation $M_{dyn} \leftrightarrow M_{stat}$ developed by Benz & Vermeer [18] is given as the light-gray range in Fig. 18. For a given M_{stat}, the correlation of Benz & Vermeer [18] predicts higher ratios M_{dyn}/M_{stat} than the correlation given in [7]. For this reason and due to the larger bandwidth, the correlation of Benz & Vermeer [18] fits better the experimental data than the correlation recommended in [7]. However, for the sands Nos. 1 and 4 some experimental data points fall below or above the range of M_{dyn}/M_{stat}-values specified by the correlation of Benz & Vermeer [18].

4.2 Correlation of M_{stat} with $G_{dyn} = G_{max}$

The determination of G_{dyn} from M_{stat} may be abbreviated by using direct correlations of both quantities. Such diagrams, showing the ratio G_{dyn}/M_{stat} as a function of M_{stat}, were derived from the experimental data and are shown in Fig. 19. The bandwidths given in Fig. 19 for different pressures and void ratios should deliver more accurate estimations of G_{dyn} than the correlation recommended in [7] in combination with an estimation of Poisson's ratio. Instead of the correlation given in [7] (or the better one proposed by Benz & Vermeer [18]), it is recommended to use the correlations shown in Fig. 19 since they are based on experimental results and distinguish with reference to the grain size distribution curve.

4.3 Correlation of E_{stat} with $E_{dyn} = E_{max}$

The original correlation of Alpan [17] is given in terms of E_{stat} and E_{dyn}. In order to prove this correlation, the monotonic triaxial test data is compared with the data from the P-wave measurements.

First, $E_{stat} = E_{50}$ is assumed. The stiffness E_{50} was obtained from the initial part of a monotonic triaxial test (Section 3.2). The corresponding mean pressure is $p = \sigma_3 + \frac{1}{3}q_{50}$ and the corresponding void ratio is $e = 0.5[e(q = 0) + e(q = q_{50})]$. For each monotonic triaxial test, using these values of e and p, the small-strain Young's modulus E_{dyn} was calculated from M_{dyn} and G_{dyn} obtained from Eqs. (7) and (8). In Fig. 20a, the ratio $E_{dyn}/E_{stat} = E_{dyn}/E_{50}$ is plotted versus $E_{stat} = E_{50}$. In contrast to the data of M_{dyn}/M_{stat} given in Fig. 18, the E_{dyn}/E_{50}-values of the four different sands presented in Fig. 20a do not differ much. The curve of Alpan [17] underestimates the experimentally obtained values E_{dyn}/E_{50} by a factor in the range between 1.5 and 2.5. Thus, the correlation of Alpan [17] delivers unrealistic estimations of the "dynamic" Young's modulus $E_{dyn} = E_{max}$, if E_{stat} is interpreted as a stiffness E_{50} for first loading.
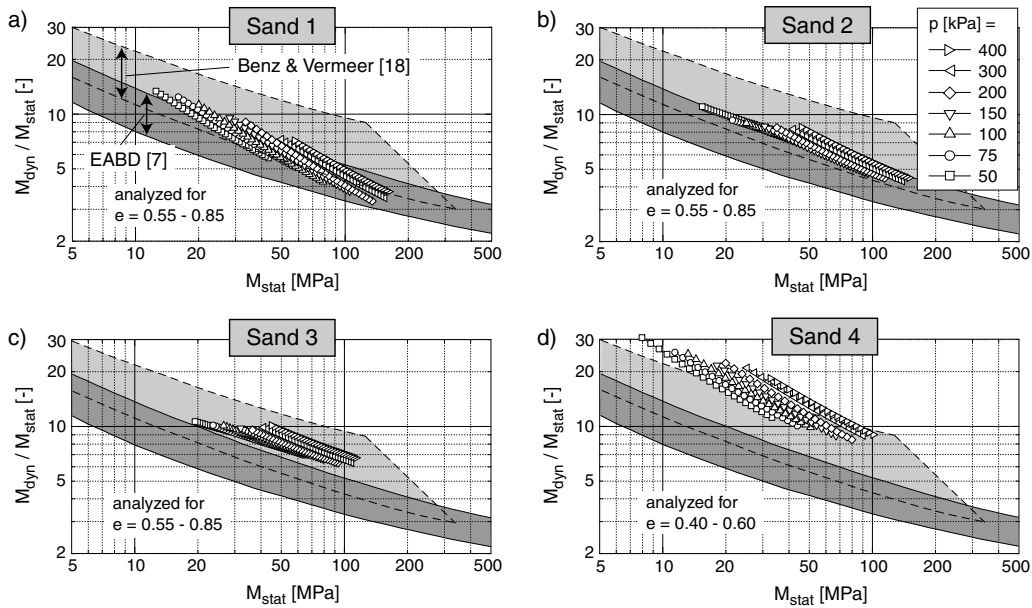
Fig. 18: *Ratio $M_{\mathrm{dyn}}/M_{\mathrm{stat}}$ as a function of M_{stat}, comparison of the experimentally obtained data with the correlations recommended in [7] and [18]*
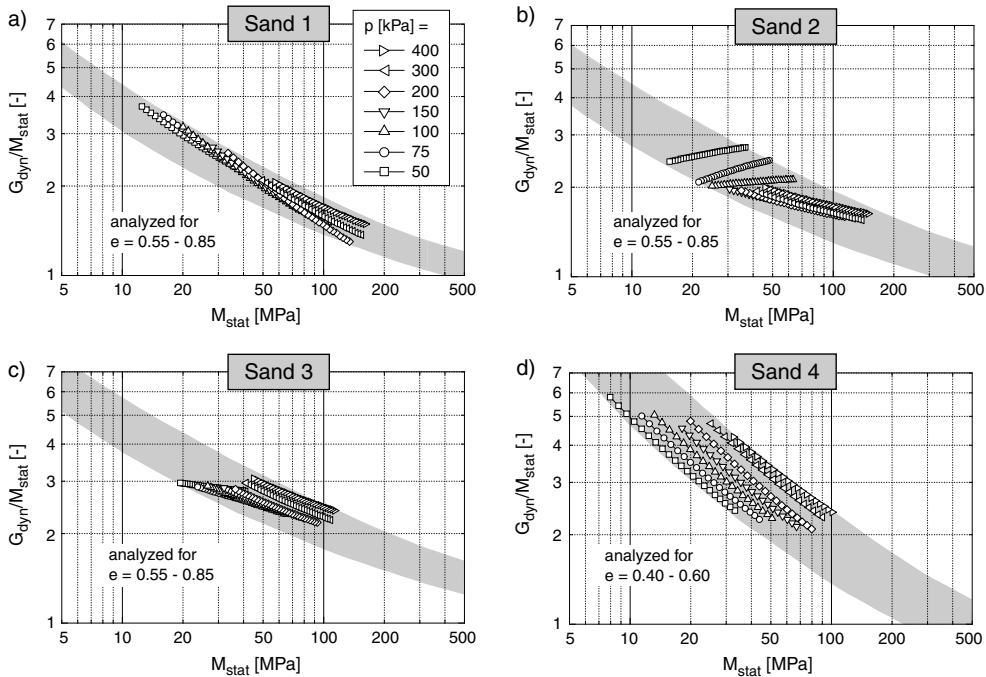

Fig. 19: *Correlation of the small-strain "dynamic" shear modulus $G_{\mathrm{max}} = G_{\mathrm{dyn}}$ with the "static" stiffness M_{stat} obtained from the first loading curve in oedometric compression tests*

Benz & Vermeer [18, 24] recommend to interpret E_{stat} as the secant modulus E_{ur} during large un- and reloading cycles in triaxial compression tests. Their assumption $E_{\mathrm{stat}} = E_{ur} = 3E_{50}$ leads to the presentation of the experimental data given in Fig. 20b (which is identical to Fig. 4 in [24]). The diagram shows the ratio E_{dyn}/E_{ur} as a function of E_{ur}. In this presentation, the experimentally obtained data coincides well with the curve proposed by Alpan [17].

Considering Figs. 18 and 20, it has to be concluded

that the experimentally obtained correlations $M_{\mathrm{dyn}} \leftrightarrow M_{\mathrm{stat}}$ and $E_{\mathrm{dyn}} \leftrightarrow E_{\mathrm{stat}}$ fit better to the curve of Alpan [17] if this curve is interpreted with $E_{\mathrm{stat}} = E_{ur} \approx 3E_{50}$ (as assumed by Benz & Vermeer [18, 24]) than with $E_{\mathrm{stat}} = E_{50}$ (as probably assumed in [7]).

However, the definition of an un- and reloading modulus for large cycles during triaxial compression seems difficult. This becomes obvious from the test results of Wu [25] presented in Fig. 21. He performed triaxial compression tests on "Karlsruher Sand" with large un- and
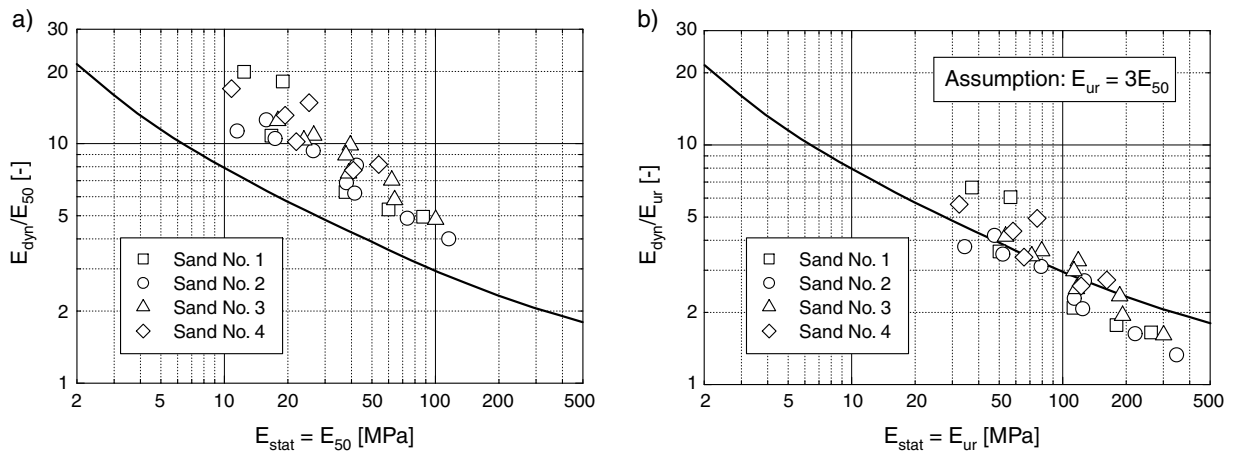
Fig. 20: *Comparison of the curve of Alpan [17] with the correlation $E_{dyn}/E_{stat} \leftrightarrow E_{stat}$ derived from the monotonic triaxial tests and the P-wave measurements: a) assuming $E_{stat} = E_{50}$, b) assuming $E_{stat} = E_{ur} = 3E_{50}$*

reloading cycles. First of all, the secant modulus E_{ur} depends on the minimum deviatoric stress q_{min} during the cycle. Considering only cycles with $q_{min} = 0$ (Fig. 21), the secant stiffness E_{ur} and thus the ratio E_{ur}/E_{50} decreases with increasing axial strain ε_1 at which the cycle is performed. This applies before and after the peak of the curve $q(\varepsilon_1)$. Furthermore, E_{ur}/E_{50} depends on the void ratio e_0, on the effective lateral stress σ_3 and on the distance $\Delta\varepsilon_1$ between two subsequent cycles. For the three tests presented in Fig. 21, E_{ur}/E_{50}-values in the range between 0.9 and 4.8 were obtained. The choice of $E_{ur}/E_{50} = 3$ seems to be a quite rough estimation, although it may be reasonable for dense sand and a relatively small axial strain ε_1 (Fig. 21).

If a more accurate correlation between E_{dyn} and E_{ur} is intended to be established based on experimental data, the performance of the un- and reloading cycles for the determination of E_{ur} has to be clearly defined (i.e. q_{min} and the axial strain ε_1 or the stress ratio $\eta = q/p$, where the unloading should commence, have to be specified).

It should be considered that E_{50} from monotonic triaxial compression tests and in particular M_{stat} from oedometric compression tests can be much easier determined in standard geotechnical laboratories than E_{ur}. Thus, correlations $M_{dyn} \leftrightarrow M_{stat}$ (Fig. 18), $G_{dyn} \leftrightarrow M_{stat}$ (Fig. 19) or $E_{dyn} \leftrightarrow E_{50}$ (Fig. 20a) will be more useful in practice than correlations $E_{dyn} \leftrightarrow E_{ur}$.

4.4 Correlation of $E_{stat} = E_{50}$ with $G_{dyn} = G_{max}$

Similar to Fig. 19 for M_{stat}, a direct correlation of the small-strain shear modulus $G_{max} = G_{dyn}$ and Young's modulus $E_{stat} = E_{50}$ from monotonic triaxial compression tests can be established. For the current test data, this correlation is shown in Fig. 22. Once again, there is no significant difference between the data for the four different sands. The data may be approximated by the average solid curve given in Fig. 22. The correlation presented in Fig. 22 may be used in practice if triaxial
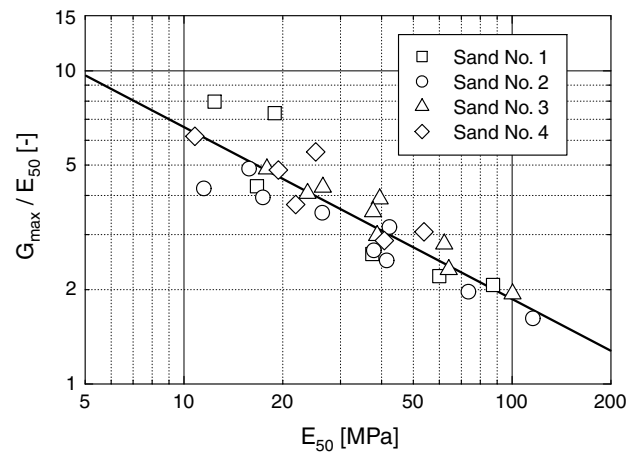
test data is available.

Fig. 22: *Correlation of the small-strain "dynamic" shear modulus $G_{max} = G_{dyn}$ with the "static" Young's modulus $E_{stat} = E_{50}$ from first loading in monotonic triaxial compression tests*

5 Summary, conclusions and outlook

The paper presents an experimental study with the aim to inspect several correlations of large-strain ("static") and small-strain ("dynamic") stiffness moduli. In particular a correlation of the constrained elastic moduli M_{stat} and $M_{dyn} = M_{max}$ is often used in practice and is critically discussed in the paper.

The modulus M_{stat} was obtained from the first loading curve in oedometric compression tests. Young's modulus $E_{stat} = E_{50}$ was derived from the initial phase of a monotonic triaxial compression test. The small-strain moduli $M_{dyn} = M_{max}$ and $G_{dyn} = G_{max}$ were obtained from P-wave measurements or resonant column tests, respectively. All types of tests were performed for four different sands with varying mean grain size $0.21 \leq d_{50} \leq 1.45$ mm and different coefficients of uniformity $1.4 \leq C_u \leq 4.5$.
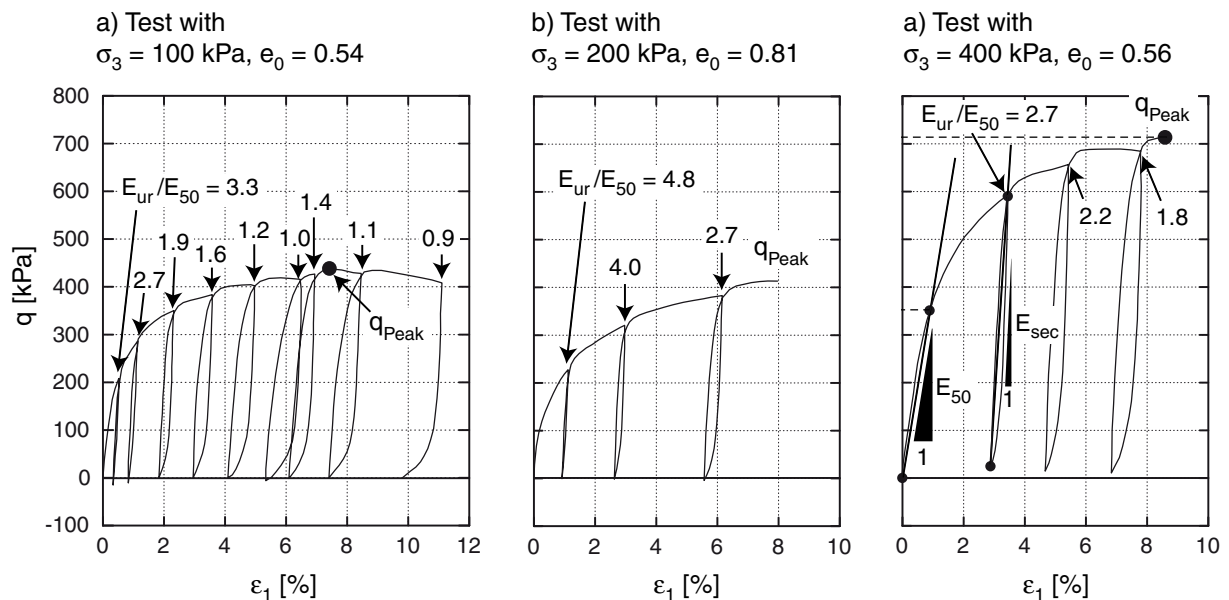
Fig. 21: *Change of the ratio E_{ur}/E_{50} during triaxial compression tests on "Karlsruher Sand" with large un- and reloading cycles performed by Wu [25]*

The analysis of the tests shows that the correlation $M_{dyn} \leftrightarrow M_{stat}$ commonly used in practice and recommended in [7] should be applied only for poorly-graded fine and medium coarse sands. It may significantly underestimate the ratio M_{dyn}/M_{stat} for poorly-graded coarse sands and for well-graded sands. A correlation recently proposed by Benz & Vermeer [18] coincides somewhat better with the experimental data. The paper also discusses the original correlation $E_{dyn} \leftrightarrow E_{stat}$ proposed by Alpan [17]. It considers different interpretations of E_{stat}.

Based on the test data, the paper proposes direct correlations between the small-strain shear modulus $G_{max} = G_{dyn}$ on one side and the stiffness M_{stat} from oedometric tests (see Fig. 19) or Young's modulus $E_{stat} = E_{50}$ from triaxial tests (see Fig. 22) on the other side. These new correlations consider the influence of the grain size distribution curve where necessary. We strongly recommend to use these new correlations for an estimation of G_{max} in practice instead of the correlation given in [7]. The new correlations are thought to be more accurate than the correlations derived theoretically from the curve of Alpan [17] using several assumptions. The present paper gives also recommendations on the choice of Poisson's ratio ν.

At present, we study the significant influence of the grain size distribution curve on the small-strain stiffness of non-cohesive soils within the framework of another research project. Up to present, more than 500 resonant column tests with additional P-wave measurements have been performed on various, specially mixed grain size distribution curves. First results concerning G_{max} have been published in [15]. It is intended to develop empirical equations for G_{max} and M_{max} which consider the influence of the grain size distribution curve. It is

expected that these formulas will deliver a better estimation of G_{max}-values for various grain size distribution curves than the correlations of "dynamic" and "static" stiffness moduli discussed in the present paper.

References

[1] A. Niemunis, T. Wichtmann, and T. Triantafyllidis. A high-cycle accumulation model for sand. *Computers and Geotechnics*, 32(4):245–263, 2005.

[2] T. Wichtmann. Explicit accumulation model for non-cohesive soils under cyclic loading. PhD thesis, Publications of the Institute of Soil Mechanics and Foundation Engineering, Ruhr-University Bochum, Issue No. 38, available from www.rz.uni-karlsruhe.de/~gn97/, 2005.

[3] T. Wichtmann, A. Niemunis, and T. Triantafyllidis. Setzungsakkumulation in nichtbindigen Böden unter hochzyklischer Belastung. *Bautechnik*, 82(1):18–27, 2005.

[4] T. Wichtmann, A. Niemunis, and T. Triantafyllidis. FE-Prognose der Setzung von Flachgründungen auf Sand unter zyklischer Belastung. *Bautechnik*, 82(12):902–911, 2005.

[5] F.E.Jr. Richart, J.R.Jr. Hall, and R.D. Woods. *Vibrations of Soils and Foundations*. Prentice-Hall, Englewood Cliffs, New Jersey, 1970.

[6] G. Gazetas. *Foundation Engineering Handbook, 2nd Edition*, chapter 15: Foundation vibrations, pages 553–593. 1991.

[7] DGGT. Empfehlungen des Arbeitskreises 1.4 "Baugrunddynamik" der Deutschen Gesellschaft für Geotechnik e.V. , 2001.

[8] B.O. Hardin and V.P. Drnevich. Shear modulus and damping in soils: design equations and curves. *Journal of the Soil Mechanics and Foundations Division, ASCE*, 98(SM7):667–692, 1972.

[9] T. Wichtmann and T. Triantafyllidis. Dynamische Steifigkeit und Dämpfung von Sand bei kleinen Dehnungen. *Bautechnik*, 82(4):236–246, 2005.

[10] S.S. Afifi and R.D. Woods. Long-term pressure effects on shear modulus of soils. *Journal of the Soil Mechanics and Foundations Division, ASCE*, 97(SM10):1445–1460, 1971.

[11] B.O. Hardin and F.E. Richart Jr. Elastic wave velocities in granular soils. *Journal of the Soil Mechanics and Foundations Division, ASCE*, 89(SM1):33–65, 1963.

[12] B.O. Hardin and W.L. Black. Sand stiffness under various triaxial stresses. *Journal of the Soil Mechanics and Foundations Division, ASCE*, 92(SM2):27–42, 1966.

[13] T. Iwasaki and F. Tatsuoka. Effects of grain size and grading on dynamic shear moduli of sands. *Soils and Foundations*, 17(3):19–35, 1977.

[14] T. Wichtmann and T. Triantafyllidis. Über den Einfluss der Kornverteilungskurve auf das dynamische und das kumulative Verhalten nichtbindiger Böden. *Bautechnik*, 82(6):378–386, 2005.

[15] T. Wichtmann, R. Martinez, F. Duran Graeff, E. Giolo, M. Navarette Hernandez, and Th. Triantafyllidis. On the influence of the grain size distribution curve on the secant stiffness of quartz sand under cyclic loading. In *11th Baltic Sea Geotechnical Conference: "Geotechnics in Maritime Engineering", Gdańsk, Poland, 15-18 September 2008*, pages 315–322, 2008.

[16] B.O. Hardin and M.E. Kalinski. Estimating the shear modulus of gravelly soils. *Journal of Geotechnical and Geoenvironmental Engineering, ASCE*, 131(7):867–875, 2005.

[17] I. Alpan. The Geotechnical Properties of Soils. *Earth Science Reviews, Elsevier*, (6):5–49, 1970.

[18] T. Benz and P.A. Vermeer. Zuschrift zum Beitrag "Über die Korrelation der ödometrischen und der "dynamischen" Steifigkeit nichtbindiger Böden" von T. Wichtmann und Th. Triantafyllidis (Bautechnik 83, No. 7, 2006). *Bautechnik*, 84(5):361–364, 2007.

[19] T. Wichtmann and Th. Triantafyllidis. Erwiderung der Zuschrift von T. Benz und P.A. Vermeer zum Beitrag "Über die Korrelation der ödometrischen und der "dynamischen" Steifigkeit nichtbindiger Böden" (Bautechnik 83, No. 7, 2006). *Bautechnik*, 84(5):364–366, 2007.

[20] G. Klein. Bodendynamik und Erdbeben. In Ulrich (eds.) Smoltczyk, editor, *Grundbautaschenbuch*, pages 443–495, 2001.

[21] *DIN 18126: Bestimmung der Dichte nichtbindiger Böden bei lockerster und dichtester Lagerung*, 1996.

[22] *E DIN 18135:1999-06 "Baugrund - Untersuchung von Bodenproben - Eindimensionaler Kompressionsversuch"*, 1999.

[23] P. Yu and F.E. Richart Jr. Stress ratio effects on shear modulus of dry sands. *Journal of Geotechnical Engineering, ASCE*, 110(3):331–345, 1984.

[24] T. Benz, R. Schwab, and P. Vermeer. Zur Berücksichtigung des Bereichs kleiner Dehnungen in geotechnischen Berechnungen. *Bautechnik*, 84(11):749–761, 2007.

[25] W. Wu. Hypoplastizität als mathematisches Modell zum mechanischen Verhalten granularer Stoffe. Veröffentlichungen des Institutes für Boden- und Felsmechanik der Universität Fridericiana in Karlsruhe, Heft Nr. 129, 1992.

Authors of this paper:

Dr.-Ing. Torsten Wichtmann, Univ.-Prof. Dr.-Ing. habil. Theodor Triantafyllidis, University of Karlsruhe, Institute for Soil Mechanics and Rock Mechanics, Engler-Bunte-Ring 14, 76131 Karlsruhe